Integration of texture analysis based on DCE-MRI K^{trans} map and metabolomics of early bone marrow microvascular changes in alloxan-induced diabetic rabbits

Yan Wang[1†], Liang Li[1†], Yuchen Yan[1], Tian Zhang[1], Lei Hu[1], Jun Chen[2] and Yunfei Zha[1*]

Abstract

Objective To evaluate early bone marrow microvascular changes in alloxan-induced diabetic rabbits using IDEAL-IQ fat quantification, texture analysis based on DCE-MRI K^{trans} map, and metabolomics.

Materials and methods 24 male Japanese rabbits were randomly divided into diabetic ($n=12$) and control ($n=12$) groups. All rabbits underwent sagittal MRI of the lumbar vertebrae at the 0th,4th, 8th, 12th, and 16th week, respectively. The fat fraction (FF) ratio and quantitative permeability of the lumbar bone marrow was measured. Texture parameters were extracted from DCE-MRI K^{trans} map. At 16th week, lumbar vertebrae 5 and 6 were used for histological analysis. Lumbar vertebra 7 was crushed to obtain bone marrow for metabolomics research.

Results The FF ratio and K^{trans} of the lumbar bone marrow in diabetic group were increased significantly at 16th week ($t=2.226$, $P=0.02$; $Z=-2.721$, $P<0.01$). Nine texture feature parameters based on DCE-MRI K^{trans} map were significantly different between the groups at the 16th week (all $P<0.05$). Pathway analysis showed that diabetic bone marrow microvascular changes were mainly related to linoleic acid metabolism. Differential metabolites were correlated with the number of adipocytes, FF ratio, and permeability parameters.

Conclusion The integration of metabolomics with texture analysis based on DCE-MRI K^{trans} map may be used to evaluate diabetic bone marrow microvascular changes at an early stage. It remains to be validated in clinical studies whether the integration of metabolomics with texture analysis based on the DCE-MRI K^{trans} map can effectively evaluate diabetic bone marrow.

Keywords Diabetes mellitus, Bone marrow, Microvascular, Magnetic resonance imaging, Metabolomics

†Yan Wang and Liang Li contributed equally to this work and share first authorship.

*Correspondence:
Yunfei Zha
zhayunfei999@126.com
[1]Department of Radiology, Renmin Hospital of Wuhan University, Wuhan 430060, China
[2]Pharmaceutical Diagnostics, GE healthcare (China), Beijing 100176, China

Introduction

Diabetes mellitus (DM) is a chronic metabolic disease. People with long-term type 1 and 2 diabetes may develop diabetic bone disorders, such as osteoporosis and osteopenia, or be at an increased risk of low-stress fractures [1, 2]. A previous study suggested that diabetic bone disease may be a chronic bone marrow microvascular complication [3]. Changes in the bone marrow microenvironment under the stimulation of high glucose promote the transformation of mesenchymal tissue into adipose tissue, inhibit the formation of osteoblasts, and cause fat accumulation in the bone marrow [4]. Hu et al. [5] found that quantitative permeability parameters of DCE-MRI and the iterative decomposition of water and fat with echo asymmetry and least-squares estimation quantitation (IDEAL-IQ) sequence can be used to quantitatively estimate changes in bone marrow microvascular permeability and fat deposition in diabetic rabbits. The advantages of quantitative permeability parameters of DCE-MRI are non-invasive and easy to operate.

Texture analysis is a method to characterize regions in an image by their texture feature in radiomics. The analysis is to quantify the intuitive textures described by terms such as silky gloss, rough, bumpy and smooth, as a function of the spatial variation in pixel intensity. Texture analysis has been of great value for the assessment of bone and muscle lesions in recent years [6]. Ito et al. [7] used computed tomography texture analysis to detect condylar bone marrow in diabetic patients. They found computed tomography texture analysis may potentially detect DM from the condylar bone marrow. Chen et al. [8] reported that texture analysis parameters based on DCE-MRI quantitative parameter K^{trans} map are feasible to identify early changes in lumbar marrow structure in diabetic rabbits.

As an emerging technology for studying small molecular metabolites, metabolomics reveals the differential metabolic pathways and potential biomarkers of disease development and provides new targets for effective early control of the disease [9]. Liquid chromatography-mass spectrometry (LC–MS) has been embraced by the metabolomics research community due to its accuracy, reproducibility, and widespread use [10]. Through the utilization of LC–MS, metabolomics can be used to identify potential biomarkers related to diseases and improve our comprehension of the disease's mechanism. As the main part of hematopoiesis, the bone marrow is composed of hematopoietic cells, adipocytes, and supportive stromal cells. As a result of aging, illness, and other factors, the elements of bone marrow can change, thus having an impact on the condition of the bone [11]. However, the mechanism of metabolic disorders in bone marrow microvascular changes remains unclear. The integration of metabolomics with texture analysis based on the volume transfer constant (K^{trans}) map to evaluate early bone marrow microvascular changes has not been reported. Therefore, we aimed to explore the feasibility of using integrated biomarkers for IDEAL-IQ, texture analysis based on the K^{trans} map, and metabolomics to evaluate early diabetic bone marrow microvascular changes.

Materials and methods

Diabetic rabbit model

The Animal Ethics Committee of Wuhan University and the Animal Experiment Centre of Renmin Hospital of Wuhan University gave authorization for all experiments, with Grant Numbers 20190421. Twenty-four Japanese male rabbits, provided by the Animal Experiment Centre of Renmin Hospital of Wuhan University, participated in this study. During a period of one week, twenty-four Japanese male rabbits, all aged between 8 and 12 weeks and weighing 3.0–3.2 kg, were introduced to a new dietary plan. Before the DM model was established, the fasting blood glucose of all the rabbits was within the normal range. For the experiment, 24 rabbits were randomly divided into two groups: a control group(n=12) and a diabetic group(n=12). The diabetic group was then given an intravenous injection of a 5% alloxan monohydrate solution (Sigma-Aldrich Chemical, 0.9% saline) via the marginal ear vein at a dosage of 100 mg/kg. To be classified as a successful diabetic rabbit model, their blood glucose concentration must reach 14 mmol/L at least once or 11 mmol/L on two occasions, 48 h apart [5, 8]. For four weeks after the diagnosis, the blood glucose concentrations of all the rabbits were monitored weekly until the condition was stabilized; the concentrations were taken before the MRI examination.

MRI examination and quantitative permeability parameters analysis

Anesthesia induction in all rabbits involved the injection of 3% pentobarbital sodium (40 mg/kg) into the marginal vein of the ear. This agent gave a rapid and powerful anesthetic effect that lasted for about 30 min. Following the successful verification of a diabetic rabbit model, a 3.0-T MR scanner (Discovery MR750 Plus, GE Healthcare, Milwaukee) and an 8-channel knee coil was employed to image the lumbar vertebrae 5–7 of the rabbits, which were anesthetized at fixed intervals (0, 4, 8, 12, and 16 weeks). To acquire anatomical images, four imaging sequences were employed: DCE-MRI, IDEAL-IQ, sagittal fast spin-echo T2-weighted imaging (FSE-T2WI), and sagittal fast spin-echo T1-weighted imaging (FSE-T1WI) (Table 1).

DCE-MRI was performed with liver acquisition volume acceleration (LAVA), using the array spatial sensitivity encoding technique. Pre-contrast LAVA series with variable flip angles used for T1 mapping (flip angles=6°, 9°,

Table 1 Imaging parameters for FSE-T1WI, FSE-T2WI, IDEAL-IQ, and DCE-MRI sequences

Sequence	Repetition time	Echo time	Flip angle	Slice thickness	Field of view	Matrix
FSE-T_1WI	300 ms	12 ms	142°	3 mm	16 cm×16 cm	320×288
FSE-T_2WI	2500 ms	120 ms	142°	3 mm	16 cm×16 cm	320×320
IDEAL-IQ	17.2 ms	1.6 ms, 3.6 ms, 5.6 ms, 7.6 ms, 9.6 ms, 11.6 ms	6°	3 mm	18 cm×0.8 cm	192×160
LAVA	3.5 ms	1.6 ms	6°, 9°, 12°	3 mm	20 cm×20 cm	192×192

12°) were performed first. Subsequently, dynamic contrast-enhanced sequences were acquired using the LAVA series (flip angle=12°) with continuous scanning for 35 phases. The contrast agent, gadodiamide (Omniscan; GE Healthcare), was injected via an intravenous catheter placed in the marginal ear vein using a contrast media injector (Medrad Spectris Solaris EP Mobile Mount MR Injection System) at a dose of 0.2 mmol/kg and flow rate of 1.0 mL/s after a 3-phase scan as baseline; this procedure was followed by a 5-mL saline flush.

Primary DCE-MRI data were analyzed using vendor-offered DCE post-processing software (Omni Kinetics, GE Healthcare). First, pre-contrast LAVA series with flip angles of 6°, 9°, and 12° were used to calculate pixel-wise T1 maps to obtain pre-contrast tissue longitudinal relaxation time. This measurement was used to convert the signal intensity units into units of contrast agent concentration. Second, the corrected 35-phase enhanced images were imported into the software. A dual-compartment extended Tofts linear model was selected to fit lumbar vertebrae 5–7 in rabbits. A circular ROI was placed in the center of the abdominal aorta to obtain the time-concentration curve as the arterial input function. The brightest phase of the lumbar central level image was selected, and the ROI was manually outlined for lumbar vertebrae 5–7, while avoiding the endplate, intervertebral disc area, vertebral venous plexus, and cerebrospinal fluid (Fig. 1). Quantitative permeability parameters, including volume transfer constant (K^{trans}), rate constant (K_{ep}), extravascular extracellular space volume fraction (V_e), and plasma volume fraction(V_p) were calculated.

Quantitative permeability parameters from the ROIs of lumbar vertebrae 5–7 were calculated based on K^{trans}, rate constant (K_{ep}), extravascular extracellular space volume fraction (V_e) and plasma volume fraction (V_p) maps shown in Fig. 1. The K^{trans} map were imported into the software (Omni Kinetics, GE Healthcare) to automatically extract 76 texture features, including grayscale histogram feature, gray level co-occurrence matrix features and gray-level run length matrix.IDEAL-IQ scan images were imported into the AW4.6 workstation (GE Healthcare). The fat fraction (FF) ratio from regions of interest (ROIs) of lumbar vertebrae 5–7 was calculated using the IDEAL IQ FF map shown in Fig. 1.

Blind to the treatment groups, two radiologists with extensive knowledge in MR diagnosis of bones and muscles, the first having three years of experience (radiologist A) and the second with five years (radiologist B), conducted all the measurements. Mean values of parameters obtained from two examiners were used for analysis. The intraclass correlation coefficient (ICC) was used to assess the agreement between radiologists A and B. The intra-observer ICC was calculated after 1 month when physician A delineated the ROI again in a different order.

Sample collection
Anesthesia induction in all rabbits involved the injection of pentobarbital sodium (100 mg/kg) into the marginal vein of the ear after MRI examination at the 16th week. Lumbar vertebrae 5 and 6 were taken for pathological examination. Lumbar vertebra 7 was crushed, and the bone marrow was frozen with liquid nitrogen and preserved at -80 °C for metabolomics.

Detection and identification of bone marrow metabolites via LC-MS
Separation and detection of bone marrow metabolites were performed using an Ultimate 3000 Accurate-Mass Q-TOF LC/MS System with Q Exactive (Thermo Fisher Scientific, USA). The samples were pretreated to obtain the supernatant (see Supplementary Material for more details). Five microliters of the supernatant sample was directly loaded onto an AQ C18 (150×2.1 mm, 1.8 μm, Ultimate) maintained at 35 ℃ by gradient elution. Mobile phase A was an acetonitrile (water [3:2] solution containing 0.1% formic acid and 10 mmol/L ammonium acetate), and mobile phase B was an isopropyl alcohol (acetonitrile [9:1] solution containing 0.1% formic acid and 10 mmol/L ammonium acetate). The flow rate was 0.3 mL min-1, with the elution gradient as follows: 0–2 min, 60–57%A; 2–2.1 min, 57–50%A; 2.1–12 min, 50–40%A; 12.0–12.1 min, 40–25%A; 12.1–18 min, 25–1%A; 18–19 min, 1%A; 19–20 min, 1–60%A; 20–25 min, 60%A.

MS spectra were acquired under negative-ion mode with the following instrument settings: detection method, full mass/dd-MS2; resolving power, 70,000 (full mass), 17,500 (dd-MS2); spray voltage, 2.8 kV; capillary temperature, 320 °C; nebulizing gas and flow rate: sheath gas and 40 Arb, respectively; and atomizer temperature, 350 °C.

Histological analysis
Lumbar vertebrae 5 and 6 were fixed with 10% paraformaldehyde. After 2 weeks of decalcification, the lumbar
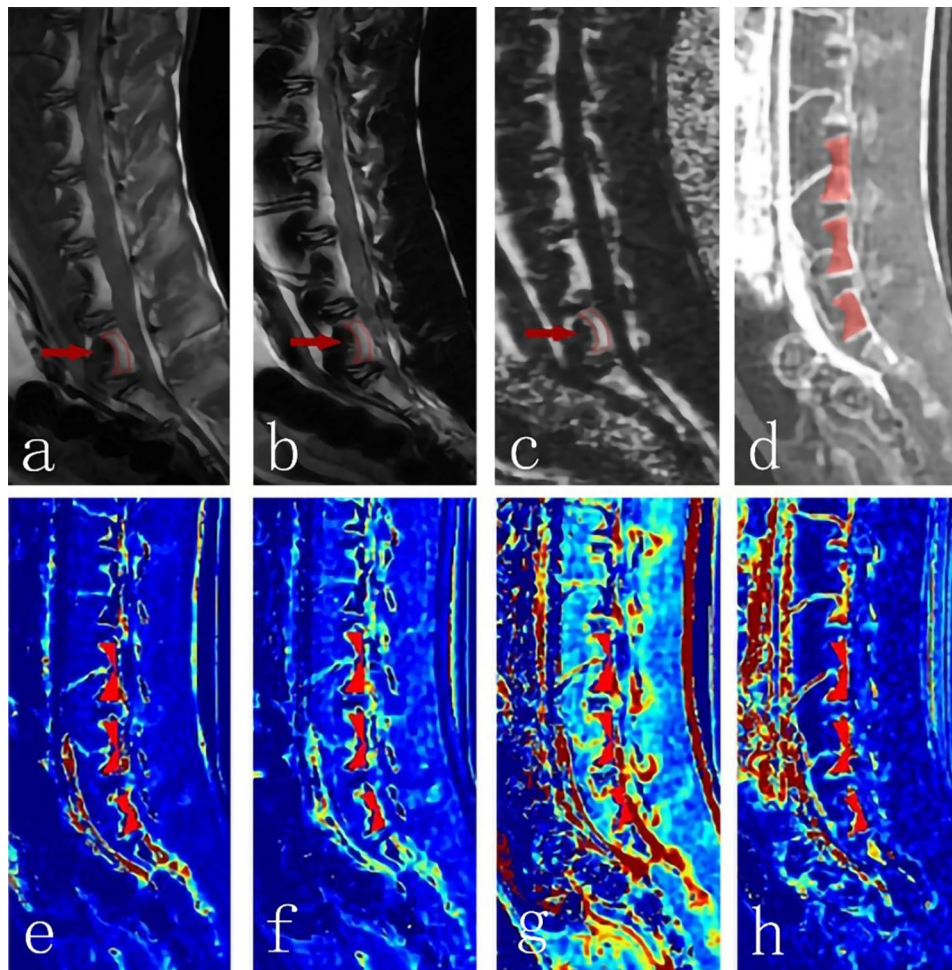
Fig. 1 Sagittal T1WI (**a**), T2WI (**b**), and FF (**c**) images of a rabbit from the diabetic group obtained at the 16th week. The ROIs (red outline) show the L7 vertebral body. DCE-MR image (**d**), K^{trans} map (**e**), K_{ep} map (**f**), V_e map (**g**), and V_p map (**h**) of a rabbit from the diabetic group obtained at the 16th week. ROIs (red outline) show the L5–7 vertebral body

vertebrae were embedded in paraffin. Four-millimeter-thick slices were obtained along the short axis of the vertebra for hematoxylin-eosin (HE) staining and CD34 immunohistochemistry.

Three discontinuous areas were randomly selected from the HE-stained sections using a light microscope with a magnification of × 200, and the number of adipocytes was counted. The average count was used as the number of adipocytes. Three independent areas of the equal area were randomly selected from HE staining sections for observation and photographing, and photographed at a magnification of × 50. Image-pro plus 6.0 (Media Cybernetics, Inc., Rockville, MD, USA) software was used to measure the trabecular area (Tb.Ar) and trabecular number (Tb.N). The average count was used as Tb.Ar and Tb.N.

The cytoplasm of vascular endothelial cells was observed to contain brownish-yellow granules indicates the presence of CD34. Upon observation, endothelial cells or clusters of endothelial cells with a

brownish-yellow hue were easily distinguishable from the surrounding microvessels and other connective tissue elements. Vascular endothelial cells or cell clusters that have obvious brownish yellow staining and can be separated from adjacent microvessels and other connective tissues can be used as single microvessels. Three discontinuous areas were randomly selected using a 200-fold light microscope, and the number of positively stained vessels was counted. The average of the measurements was used as the microvessel density (MVD).

Statistical analyses

After the bone marrow metabolite assessment, LC-MS data were preprocessed using MSDIAL software. Details are available in the Supplementary Material. Using R studio (version 4.0.3), pathway analysis was performed using enrichment analysis and topology analysis to identify differential metabolic pathways and differential metabolites that were significantly different in the diabetes group.

Data were statistically analyzed using IBM SPSS ver. 26.0. The FF ratio and DCE-MRI quantitative permeability parameters were tested for normality, followed by homogeneity test for variance. Data are presented as mean±standard deviation. The independent sample t-test or Mann-Whitney U test was used to compare DCE-MRI quantitative permeability parameters, FF ratios at the same time point, MVD, and number of adipocytes, Tb.Ar and Tb.N at the 16th week in the groups. DCE-MRI quantitative permeability parameters and FF ratios at different time points in the same group were compared using repeated-measures analysis of variance. Regarding texture analysis, two-step analysis algorithms were used to assess texture features at the 16th week. First, differences between texture features of the two cohorts were assessed with ANOVA or Mann-Whitney U test, according to the distribution of the data. Univariate logistic regression was used to analyze the remaining texture features.

Spearman correlation coefficients were used to evaluate correlations between MVD, number of adipocytes, Tb.Ar, Tb.N, FF ratio, DCE-MRI quantitative permeability parameters, texture feature parameters, and differential metabolites of lumbar bone. $P < 0.05$ denoted statistical significance.

Results

In the diabetic group, one rabbits died because of poor health conditions and one rabbit failed to maintain a hyperglycemic state. In the control group, two rabbits died owing to an anesthetic accident.

Analysis of MRI quantitative parameters

The inter- and intra-observer ICCs (0.80–0.92; $P < 0.01$) of the measured values of MRI quantitative parameters indicated good consistency. The FF ratio and K^{trans} in the diabetic group were greatly higher at the 16th week than at the 0th, 4th, 8th and 12th week (all $P < 0.05$). There were significant differences in the FF ratio, K^{trans}, and V_e between the diabetic and control groups at the 16th

week ($t = 2.226$, $P = 0.02$; $Z = -2.721$, $P < 0.01$; $Z = -2.192$, $P = 0.028$) (Supplementary Table 1, Supplementary Fig. 1).

Texture analysis based on DCE-MRI K^{trans} map

The inter- and intra-observer ICCs (0.80–0.92; $P < 0.01$) of the measured values of texture features based on the K^{trans} map indicated good consistency. Twenty-five features were selected by ANOVA and Mann-Whitney U test during texture analysis based on the K^{trans} map at the 16th week. The nine features were further screened by univariate logistic regression analysis among the twenty-five features, including mean deviation, quantile50, quantile75, quantile95, RMS, sum average, difference entropy, and mean value (Table 2).

Metabolic profiling of bone marrow of lumbar vertebra 7

LC-MS was performed on the bone marrow of lumbar vertebra 7 in all experimental rabbits. The principal component analysis(PCA)and partial least squares discriminant analysis (PLS-DA) plots show that show the tendency for the diabetic group to be separate from the control group (Fig. 2). The R^2 of the PLS-DA model was 80%, while the Q^2 of the PLS-DA model was 10%. Based on variable importance in the projection scores>1 and fold change scores>2 or <0.5, we screened 36 differential metabolites in Fig. 3. Pathway analysis was performed using enrichment analysis and topology analysis to identify differential metabolic pathways. As summarized in Table 3, the differential metabolic pathways related to bone marrow microvascular changes included linoleic acid metabolism, arachidonic acid metabolism, fatty acid biosynthesis, fatty acid elongation, fatty acid degradation, histidine metabolism, beta-alanine metabolism, alpha-linolenic acid metabolism, glycosylphosphatidylinositol-anchor biosynthesis, purine metabolism, and glycerophospholipid metabolism. These results suggest a significant perturbation in lipid fluxes. Because the p-value of linoleic acid metabolism is low, which indicated statistical significance, and the impact score is high, we then focus on linoleic acid metabolism. Five differential metabolites, including four phosphatidylcholines

Table 2 Univariate logistic regression results for texture features based on the K^{trans} map at the 16th week

Texture variable	Diabetic group	Control group	β(95%CI)	*P*-value
Median intensity	0.509±0.302	0.109±0.137	9.206(0.598,17.814)	0.036
Mean deviation	254.309±0.407	254.785±0.157	-7.296(-14.325,-0.267)	0.041
Quantile50	0.502±0.298	0.110±0.135	9.294(0.667, 17.92)	0.034
Quantile75	1.004±0.639	0.247±0.204	6.519(0.236, 12.802)	0.041
Quantile95	1.887±1.123	0.675±0.469	2.444(0.097, 4.791)	0.041
RMS	0.957±0.578	0.406±0.298	3.169(0.004, 6.335)	0.049
Sum average	0.147±0.055	0.074±0.065	20.425(1.136, 39.713)	0.037
Difference entropy	0.601±0.076	0.434±0.185	12.810(0.007, 25.613)	0.049
Mean value	0.690±0.408	0.215±0.157	7.267(0.262, 14.271)	0.042

Abbreviation: β, unstandardized regression coefficient; CI, confidence interval
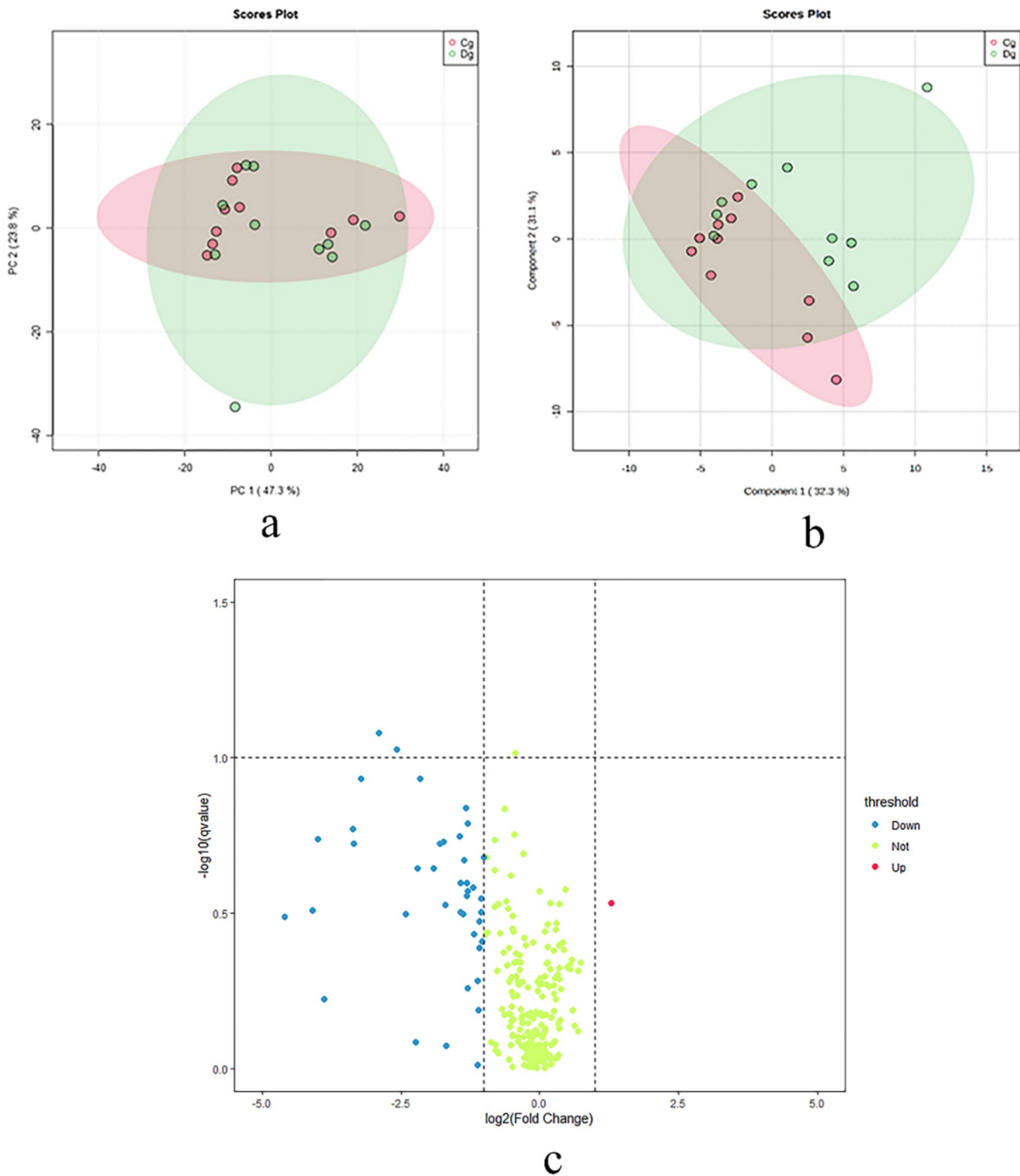
Fig. 2 Metabolomic analysis and identification of differential metabolites. PCA and PLS-DA plots show the tendency for the diabetic group (Dg, green circles and green ellipses) to be separate from the control group (Cg, red circles and red ellipses) (**2a**, **b**). A volcano plot showing the distribution of all and differential metabolites based on their fold-change values (x-axis, logarithmic scale) and *p*-values (y-axis, logarithmic scale) (**2c**)

(PCs) and one fatty acid, were related to linoleic acid metabolism and were selected for further correlation analysis. They were PC 14:0–16:0, PC 15:0–18:1, PC 18:0–20:2, PC 18:1–20:1, and FA 18:2.

Histological results

CD34 immunohistochemical staining showed that the MVD in the diabetic group was lower than that in the control group at the 16th week ($Z=-3.785$, $P<0.01$). HE
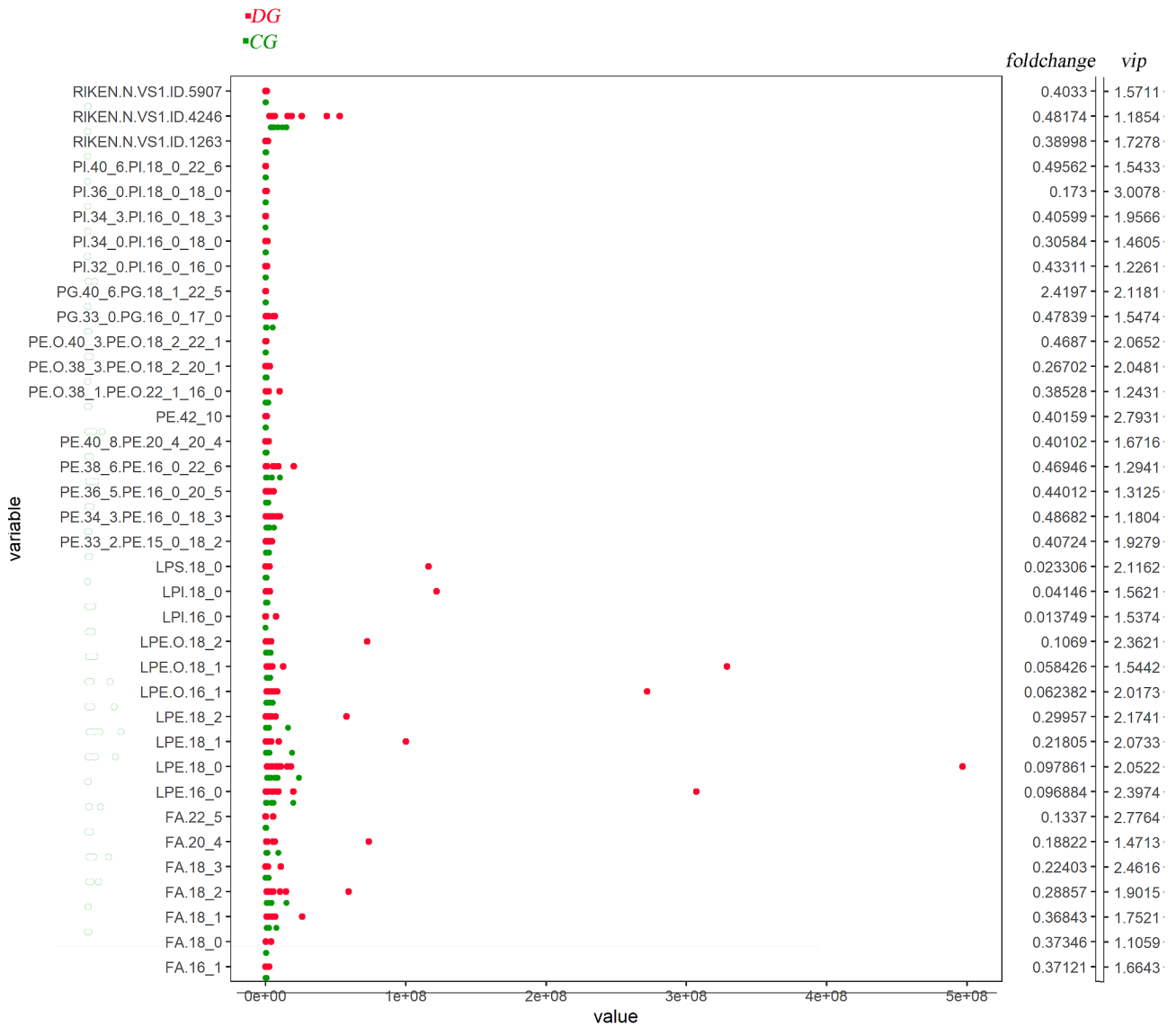
Fig. 3 Summary of all 36 differential metabolites, their respective fold-change values and VIP as calculated by R studio. Each red and green dot represent the diabetic group and the control group, respectively. The average fold-change and VIP of each metabolite in diabetic group or the control group is denoted by a vertical line

Table 3 Enriched metabolic pathways from differential metabolites

Name	Total	Hits	Raw P	Impact
Linoleic acid metabolism	5	2	0.25148	0.96774
Arachidonic acid metabolism	36	2	0.33321	0.28076
Fatty acid biosynthesis	46	1	0.36874	0
Fatty acid elongation	38	1	0.36874	0
Fatty acid degradation	39	1	0.36874	0
Histidine metabolism	15	1	0.37446	0
Beta-alanine metabolism	19	1	0.37446	0
Alpha-linolenic acid metabolism	13	2	0.39292	0.32258
Glycosylphosphatidylinositol-anchor biosynthesis	15	1	0.40829	0
Purine metabolism	66	1	0.436	0.0011005
Glycerophospholipid metabolism	36	3	0.49024	0.26382

staining showed that the number of adipocytes in the diabetic group was higher than that in the control group ($t=1.125$, $P=0.037$) (Fig. 4). HE staining of the lumbar spine in the diabetic group showed a decrease in the area and number of trabecular bone(Figure 5). The Tb.Ar and Tb.N in the diabetic group were lower than those in the control group ($t=-4.540$, $P=0.016$; $t=-2.827$, $P=0.043$).

Correlation analysis

In Fig. 6, spearman correlation analysis showed that MVD was negatively correlated with median intensity, quantile50, and quantile75 ($r=-0.504$, $P=0.023$; $r=-0.490$, $P=0.028$; $r=-0.541$, $P=0.014$; 95% *CI*). The number of adipocytes was negatively correlated with

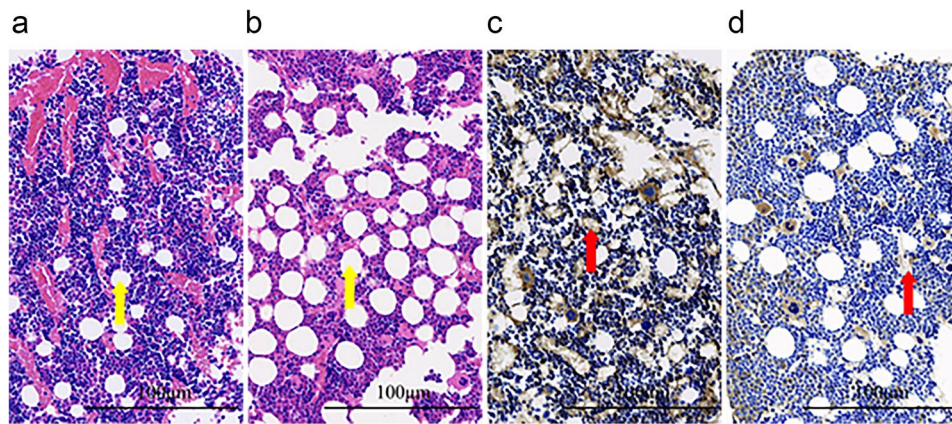Wang *et al. BMC Medical Imaging*   (2024) 24:247

Page 8 of 11

Fig. 4 Decrease in the number of adipocytes (yellow arrow) in the control group (**4a**). Increase in the number of adipocytes (yellow arrow) in the diabetic group (**4b**) (HE staining; original magnification, ×200). Microvessels (red arrow) are sparser in the diabetic group (**4d**) than in the control group (**4c**) (CD34 staining; original magnification, ×200)
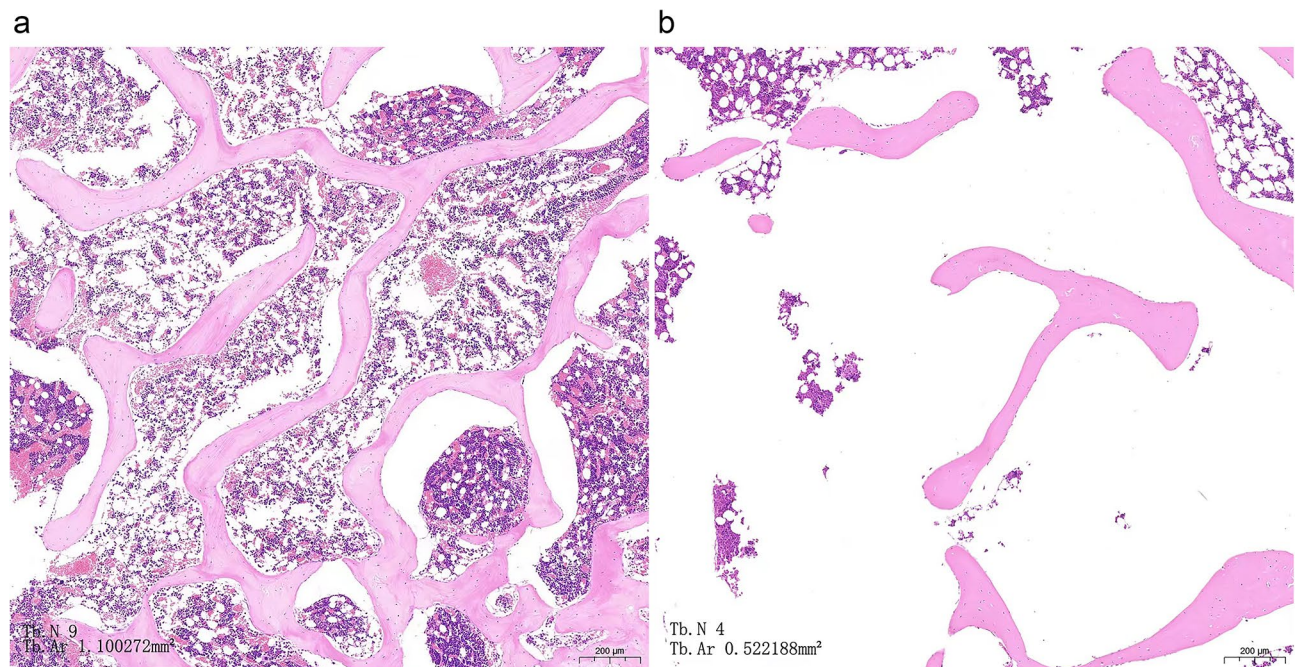

Fig. 5 The Tb.Ar and Tb.N in the diabetic group (**5b**) were lower than those in the control group (**5a**) (HE staining; original magnification, ×50)

PC 14:0–16:0 and PC 18:1–20:1 (r=-0.501, P=0.025; r=-0.467, P=0.038; 95% *CI*). The FF ratio was positively correlated with PC 15:0–18:1 (r=-0.457, P=0.043; 95% *CI*), and K_{ep} was negatively correlated with PC 14:0–16:0 (r=-0.478, P=0.033, 95% *CI*). The correlations between the remaining parameters were not statistically significant (P>0.05).

Discussion

To our knowledge, this is the first study to evaluate early bone marrow microvascular changes in alloxan-induced diabetic rabbits using texture analysis based on the K^{trans} map and metabolomics. Using metabolomics, we identified 36 metabolites that exhibited differential levels between diabetic group and control group. Using pathway analysis we found that early diabetic bone marrow microvascular changes were related to a lipid metabolism disorder, which was mainly related to linoleic acid metabolism.

In this study, the FF ratio in the diabetic group was significantly higher at the 16th week, which was in accordance with the findings of Hu et al. [5]. Adipocytes or osteoblasts can be differentiated from mesenchymal stem cells (MSCs) in the bone marrow [12]. The mechanism underlying the increase in bone marrow fat content may be a change in the bone marrow microenvironment caused by a high glucose environment, which can induce the differentiation of intra-marrow MSCs into
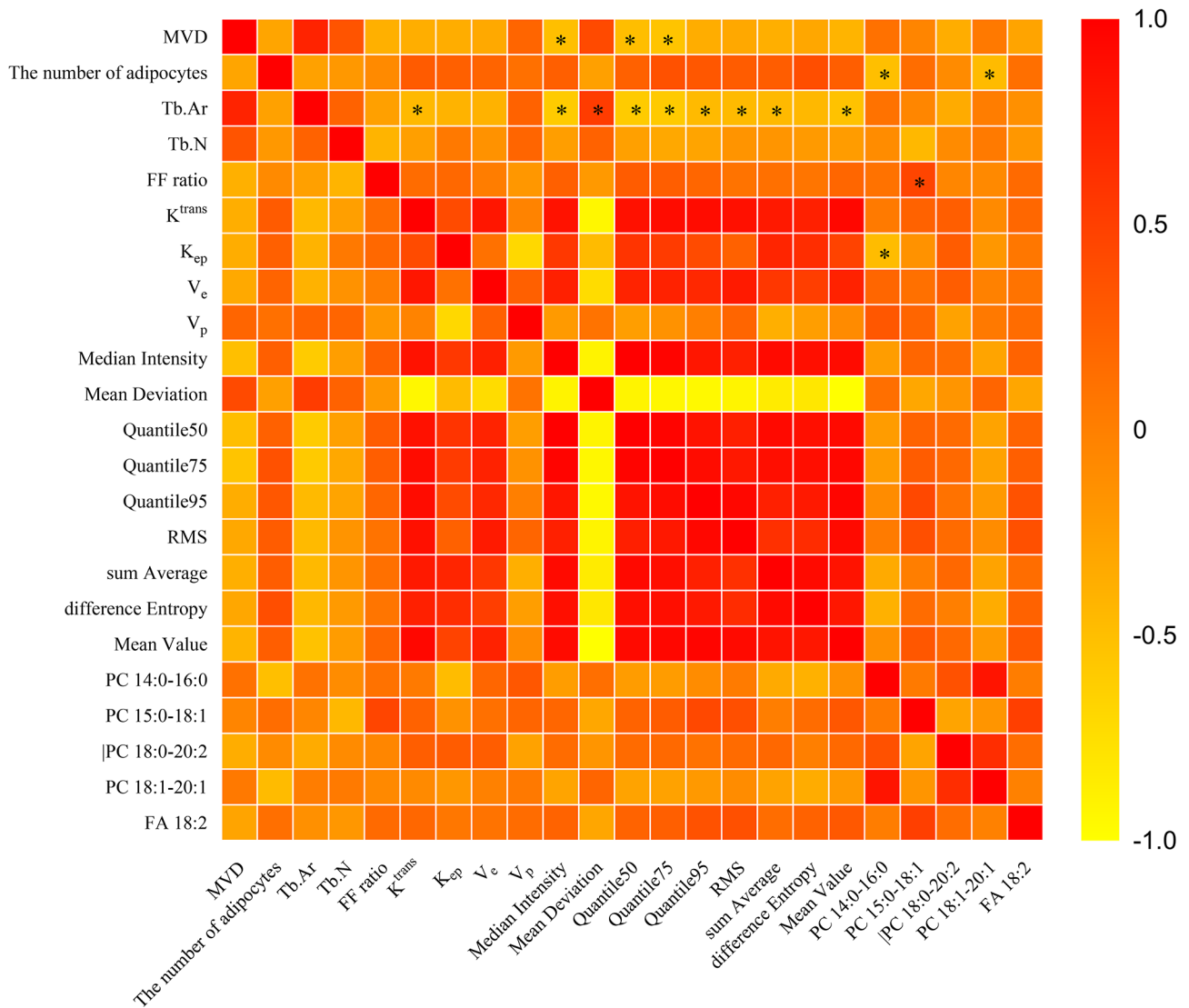
Fig. 6 Correlation heat map of histological data, imaging data and differential metabolites. *represents *P*<0.05. Color bar represents the *r* value

adipocytes, leading to an growth in fat content. K^{trans} represents the contrast dose of the contrast agent from the blood vessel to the extracellular space within a unit of time. We found that K^{trans} of the diabetic group was significantly higher at the 16th week, indicating an increase in bone marrow microvascular permeability during the early stages of diabetes, which was in accordance with the results of previous studies [13]. Otherwise, the MVD in the diabetic group was lower at the 16th week. This reduction in microvasculature may indicate the disruption of endothelial function. Endothelial dysfunction can give rise to enhanced microvascular permeability, which may be one of the reasons for the increase of K^{trans} value.

The following nine texture feature parameters based on the K^{trans} map were statistically different in two groups at the 16th week: median intensity, mean deviation, quantile50, quantile75, quantile95, RMS, sum average,

difference entropy, and mean value. This suggests that texture analysis based on the K^{trans} map may be sensitive for detecting alterations in the microarchitecture of diabetic bone marrow. In addition, MVD was correlated with texture feature parameters, demonstrating that microvascular changes affected the bone marrow microstructure, which ultimately led to changes in bone marrow texture parameters. This finding was in accordance with Yang et al [14].

In our study, we found that diabetic bone marrow microvascular changes were related to lipid metabolism disorder, which was mainly related to linoleic acid metabolism. Previous studies reported that linoleic acid metabolism disorder was related to diabetic retinopathy and diabetic kidney disease [15, 16]. Diabetic retinopathy and diabetic kidney disease are part of diabetic microvascular disease. Our study revealed for the first time that diabetic

bone marrow microvascular changes were mainly related to changes in the linoleic acid metabolism pathway. As numerous studies have demonstrated, Linoleic acid, a type of polyunsaturated fatty acid (PUFA), has a direct impact on metabolism, largely as a result of its effects on inflammation and oxidative stress [16]. Hyperosmolar stress and the activation of inflammatory pathways, as well as oxidative have been recognized as key underlying events in diabetic microvascular disease [17]. In addition, It has been demonstrated in prior research that alterations in polyunsaturated fatty acid levels can result in disruptions of endothelial function due to their effect on the quantity and performance of endothelial progenitor cells [18, 19]. Endothelial dysfunction is the central link in the occurrence and progress of diabetic microvascular complications in multiple target organs [20, 21]. Bellissimo et al. [22] reported that pathways related to fatty acid metabolism, especially the n-6 fatty acid linoleic acid, were significantly relevant with bone mineral density based on the results of plasma high-resolution metabolomics. Metabolic products of linoleic acid, which include arachidonic acid, hydroxyoctadecadienoic acid (HODE), and epoxyoctadecenoic acid/hydroperoxy-octadecadienoic acid, are associated with bone health. As the main precursor of the pro-inflammatory eicosanoid pathway, Arachidonic acid is proposed to be responsible for the formation of osteoclasts [23–25] and the resorption of bone in human bone marrow cultures via prostaglandin E2 [26]. Oxylipins, such as 9-HODE and 13-HODE, which are derived from linoleic acid, act as agonists of the peroxisome proliferator-activated receptor-gamma, stimulating the differentiation of mesenchymal stem cells into adipocytes and inhibiting the differentiation of osteoblast [27, 28]. Metabolites related to the linoleic acid pathway may be the potential biomarkers for early diabetes-related bone marrow microvascular changes.

Differential metabolites, also referred to as metabolites related to the linoleic acid pathway, were correlated with the number of adipocytes, FF ratio, and permeability parameters. Since the FF ratio, and permeability parameters were confirmed to be related to the early microvascular changes in the diabetic bone marrow [5]. Thus, our findings indicate that changes in fat and microvascular permeability of the bone marrow of the lumbar vertebra were related to linoleic acid metabolism. Monitoring FF ratio, permeability parameters and the concentrations of metabolites related to the linoleic acid pathway may facilitate the prediction and early diagnosis of early microvascular changes in the diabetic bone marrow. The further research on mechanism need be carried out to elucidate the exact role of linoleic acid on microvascular changes in the diabetic bone marrow. However, our study showed no association between differential metabolites and texture feature parameters. The reason may be that the data

structures and types of radiomics and metabolomics are different. Different omics data also lead to different evaluation models. How to use efficient and effective integration methods or algorithm models to integrate different omics data and mine the hidden information in multiomics data is an urgent problem to be solved.

This study has several limitations. First, the progress of diabetes was observed only for 16 weeks, which was different from the natural course of patients with clinical diabetes. Second, our study did not reveal the time sequence of each parameter change. Finally, the technology of metabolomics has not yet been perfected to confirm all the metabolites involved in diabetic myelopathy, and the accuracy of detection still needs to be improved.

Conclusion

In conclusion, the integration of metabolomics with texture analysis based on the DCE-MRI K^{trans} map may be used to evaluate diabetic bone marrow. It remains to be validated in clinical studies whether the integration of metabolomics with texture analysis based on the DCE-MRI K^{trans} map can effectively evaluate diabetic bone marrow.

Abbreviations

DM	Diabetes mellitus
DCE-MRI	Dynamic contrast-enhanced magnetic resonance imaging
IDEAL-IQ	The iterative decomposition of water and fat with echo asymmetry and least-squares estimation quantitation
K^{trans}	Volume transfer constant
FSE-T1WI	Sagittal fast spin-echo T1-weighted imaging
FSE-T2WI	Sagittal fast spin-echo T2-weighted imaging
FF	Fat fraction
ROI	Region of interest
K_{ep}	Rate constant extravascular
V_e	Extracellular space volume fraction
V_p	Plasma volume fraction
ICC	Intraclass correlation coefficient
LC-MS	Liquid chromatography-mass spectrometry analysis
HE	Hematoxylin-eosin
Tb.Ar	Trabecular area
Tb.N	Trabecular number
MVD	Microvessel density
PCA	Principal component analysis
PLS-DA	Partial least squares discriminant analysis
PC	Phosphatidylcholine
MSC	Mesenchymal stem cell
HODE	Hydroxyoctadecadienoic acid

Supplementary Information

The online version contains supplementary material available at https://doi.org/10.1186/s12880-024-01416-z.

Supplementary Material 1

Author contributions

YW, LL and YFZ participated in the study design, evaluated the results, and wrote the frst and revised manuscript. YCY, TZ, LH and JC implemented the

methods and performed the data analysis. All authors read and approved the manuscript.

Data availability
The raw data may be made available upon reasonable request from the corresponding author.

Declarations

Ethics approval and consent to participate
All experimental protocols were approved by the Animal Ethics Committee of Wuhan University (Grant Numbers 20190421). Clinical trial number: not applicable.

Consent for publication
Not applicable.

Competing interests
One author of this manuscript (Jun Chen) is an employee of GE Healthcare. The remaining authors declare no affiliation with any company whose products or services may be relevant to the subject of this article.

References

1. Dumitru N, Carsote M, Cocolos A, Petrova E, Olaru M, Dumitrache C, Ghemigian A. The link between bone osteocalcin and energy metabolism in a group of postmenopausal women. Curr Health Sci J. 2019;45(1):47–51. https://doi.org/10.12865/CHSJ.45.01.06
2. Ebrahimpur M, Sharifi F, Nezhad FA, Bagherzadeh M, Ostovar A, Shafiee G, Heshmat R, Mehrdad N, Razi F, Khashayar P, Nabipour I, Larijani B. Effect of diabetes on BMD and TBS values as determinants of bone health in the elderly: Bushehr Elderly Health program. J Diabetes Metab Disord. 2019;18(1):99–106. https://doi.org/10.1007/s40200-019-00395-1
3. Shanbhogue VV, Hansen S, Frost M, Brixen K, Hermann AP. Bone disease in diabetes: another manifestation of microvascular disease? Lancet Diabetes Endocrinol. 2017;5(10):827–38. https://doi.org/10.1016/S2213-8587(17)30134-1
4. Murray CE, Coleman CM. Impact of diabetes mellitus on bone health. Int J Mol Sci. 2019;20(19):4873. https://doi.org/10.3390/ijms20194873
5. Hu L, Zha YF, Wang L, Li L, Xing D, Gong W, Wang J, Lin Y, Zeng FF, Lu XS. Quantitative evaluation of vertebral microvascular permeability and fat fraction in alloxan-induced diabetic rabbits. Radiology. 2018;287(1):128–36. https://doi.org/10.1148/radiol.2017170760
6. Chen PP, Zha YF. Research progress of radiomics in musculoskeletal diseases. Chin J Radiol. 2019;53(9):794–6. https://doi.org/10.3760/cma.j.issn.1005-1201.2019.09.020. (in Chinese).
7. Ito K, Muraoka H, Hirahara N, Sawada E, Okada S, Kaneda T. Computed tomography texture analysis of mandibular condylar bone marrow in diabetes mellitus patients. Oral Radiol. 2021;37(4):693–9.
8. Chen P, Zha Y, Wang L, Li L, Hu L, Xing D, Liu B, Yang L, Yang Q, Liu C, Liu H, Liu W. Evaluation of bone marrow texture and trabecular changes with quantitative DCE-MRI and QCT in Alloxan-Induced Diabetic rabbit models. Front Endocrinol (Lausanne). 2021;12:785604.
9. Jin Q, Ma RCW. Metabolomics in diabetes and diabetic complications: insights from epidemiological studies. Cells. 2021;10(11):2832. https://doi.org/10.3390/cells10112832
10. Chen CJ, Lee DY, Yu J, Lin YN, Lin TM. Recent advances in LC-MS-based metabolomics for clinical biomarker discovery. Mass Spectrom Rev. 2022;e21785. https://doi.org/10.1002/mas.21785
11. Li X, Wang Y, Gao M, Bao B, Cao Y, Cheng F, Zhang L, Li Z, Shan J, Yao W. Metabolomics-driven of relationships among kidney, bone marrow and bone of rats with postmenopausal osteoporosis. Bone. 2022;156:116306. https://doi.org/10.1016/j.bone.2021.116306
12. Muruganandan S, Govindarajan R, Sinal CJ. Bone marrow adipose tissue and skeletal health. Curr Osteoporos Rep. 2018;6(4):434–42. https://doi.org/10.1007/s11914-018-0451-y
13. Shi Y, Vanhoutte PM. Macro- and microvascular endothelial dysfunction in diabetes. J Diabetes. 2017;9(5):434–49. https://doi.org/10.1111/1753-0407.12521
14. Yang L, Li D, Yan Y, Yang Q, Li L, Zha Y. Microvascular permeability and texture analysis of bone marrow in diabetic rabbits with critical limb ischemia based on dynamic contrast-enhanced magnetic resonance imaging. J Diabetes Investig. 2024;15(5):584–93. https://doi.org/10.1111/jdi.14145
15. Zuo J, Lan Y, Hu H, Hou X, Li J, Wang T, Zhang H, Zhang N, Guo C, Peng F, Zhao S, Wei Y, Jia C, Zheng C, Mao G. Metabolomics-based multidimensional network biomarkers for diabetic retinopathy identification in patients with type 2 diabetes mellitus. BMJ Open Diabetes Res Care. 2021;9(1):e001443. https://doi.org/10.1136/bmjdrc-2020-001443
16. Zhang H, Zuo JJ, Dong SS, Lan Y, Wu CW, Mao GY, Zheng C. Identification of potential serum metabolic biomarkers of diabetic kidney disease: A widely targeted metabolomics study. J Diabetes Res. 2020; 2020:3049098. https://doi.org/10.1155/2020/3049098
17. Madonna R, Balistreri CR, Geng YJ, De Caterina R. Diabetic microangiopathy: pathogenetic insights and novel therapeutic approaches. Vascul Pharmacol. 2017;90:1–7. https://doi.org/10.1016/j.vph.2017.01.004
18. Rodríguez C, Slevin M, Rodríguez-Calvo R, Kumar S, Krupinski J, Tejerina T, Martínez-González J. Modulation of endothelium and endothelial progenitor cell function by low-density lipoproteins: implication for vascular repair, angiogenesis and vasculogenesis. Pathobiology. 2009;76(1):11–22. https://doi.org/10.1159/000178151
19. Ghosh A, Gao L, Thakur A, Siu PM, Lai CWK. Role of free fatty acids in endothelial dysfunction. J Biomed Sci. 2017;24(1):50. https://doi.org/10.1186/s12929-017-0357-5
20. Yiu KH, Tse HF. Specific role of impaired glucose metabolism and diabetes mellitus in endothelial progenitor cell characteristics and function. Arterioscler Thromb Vasc Biol. 2014;34(6):1136–43. https://doi.org/10.1161/ATVBAHA.114.302192
21. Tsukada S, Masuda H, Jung SY, Yun J, Kang S, Kim DY, Park JH, Ji ST, Kwon SM, Asahara T. Impaired development and dysfunction of endothelial progenitor cells in type 2 diabetic mice. Diabetes Metab. 2017;43(2):154–62. https://doi.org/10.1016/j.diabet.2016.07.034
22. Bellissimo MP, Ziegler TR, Jones DP, Liu KH, Fernandes J, Roberts JL, Weitzmann MN, Pacifici R, Alvarez JA. Plasma high-resolution metabolomics identifies linoleic acid and linked metabolic pathways associated with bone mineral density. Clin Nutr. 2021;40(2):467–75. https://doi.org/10.1016/j.clnu.2020.05.041
23. Gabbs M, Leng S, Devassy JG, Monirujjaman M, Aukema HM. Advances in our understanding of oxylipins derived from dietary PUFAs. Adv Nutr. 2015;6(5):513–40. https://doi.org/10.3945/an.114.007732
24. Innes JK, Calder PC. Omega-6 fatty acids and inflammation. Prostaglandins Leukot Essent Fat Acids. 2018;132:41–8. https://doi.org/10.1016/j.plefa.2018.03.004
25. Wang W, Zhu J, Lyu F, Panigrahy D, Ferrara KW, Hammock B, Zhang G. ω-3 polyunsaturated fatty acids-derived lipid metabolites on angiogenesis, inflammation and cancer. Prostaglandins Other Lipid Mediat. 2014;113–115:13–20. https://doi.org/10.1016/j.prostaglandins.2014.07.002
26. Longo AB, Ward WE. PUFAs, bone mineral density, and fragility fracture: findings from human studies. Adv Nutr. 2016;7(2):299–312. https://doi.org/10.3945/an.115.009472
27. Lecka-Czernik B, Moerman EJ, Grant DF, Lehmann JM, Manolagas SC, Jilka RL. Divergent effects of selective peroxisome proliferator-activated receptor-gamma 2 ligands on adipocyte versus osteoblast differentiation. Endocrinology. 2002;143(6):2376–84. https://doi.org/10.1210/endo.143.6.8834
28. Lin SJ, Yang DR, Yang G, Lin CY, Chang HC, Li G, Chang. C.TR2 and TR4 orphan nuclear receptors: an overview. Curr Top Dev Biol. 2017;125:357–73. https://doi.org/10.1016/bs.ctdb.2017.02.002